



Micro Gravity Balloon Drop: Tether Release

Natalie A. Ramm¹ and Bill G. Solyst²
Taylor University, Upland, IN, 46989

Ben C. Fisher³ and Reid E. Dodge⁴
Taylor University, Upland, IN, 46989

and

Anthony J. Pollina⁵ and Paul G. Kuehl⁶
Taylor University, Upland, IN, 46989

The main objective of this balloon launch is to test the release of a ten meter boom in microgravity (free fall) at 25 km altitude. The successful release and unraveling of the tether will be a monumental achievement in the area of Pico-Satellite capabilities. In addition to the ten meter boom, a new design of inserting a smaller balloon inside of the parachute for a less chaotic decent in free fall has been implemented with success. Microgravity is an important environment for experimentation. There is a short period of microgravity after the payload is dropped before resistive forces become significant. Microgravity gives an opportunity to test equipment in roughly zero Gs with only a few percent of the Earth's atmosphere. This project tests a real mass model satellite and attempts to optimize a balloon launch for space environment testing.

Other important experiments included in this launch consist of the GaAs Solar Array Testing, Thermal Surface Model Testing, Communications link testing with a new nickel-titanium wire J-pole antenna and a Tether Release Model computer simulation that will be compared to the actual experimental execution of the tether release.

Nomenclature

A	= area, Ampere unit of current
B	= magnetic field
d	= diameter
ϵ	= emissivity
g	= grams, unit of mass, also kilo-grams (kg) =1000g, g also represents gravity and a unit of acceleration.
h	= height
I	= current, inertia
L	= length
m	= meters, unit of length, also in kilo-meters (km)
Ω	= ohms, unit of resistance
P	= Power
r	= radius
R	= resistance, Ideal Gas Constant = $8.314 \frac{\text{Pa}\cdot\text{m}^3}{\text{mol}\cdot\text{K}}$
σ	= Stefan-Boltzmann constant
T	= Tesla unit of magnetic field, Temperature
V	= volume, Volts, Voltage

¹ Research Intern, Department of Physics and Engineering, 236 W. Reade Ave., and Student- New.

² Student, Department of Physics and Engineering, 236 W. Reade Ave.

³ Student, Department of Physics and Engineering, 236 W. Reade Ave.

⁴ Student, Department of Physics and Engineering, 236 W. Reade Ave.

⁵ Student, Department of Physics and Engineering, 236 W. Reade Ave.

⁶ Student, Department of Physics and Engineering, 236 W. Reade Ave.

I. Introduction

In this balloon launch a real mass model of ESAT, a low orbit Pico-Satellite designed at Taylor University, (Cattrell et. al. 2011) will be used. Being tested is a release mechanism and unraveling of a ten meter boom. ESAT and its subsystems will be tested in a variety of ways. ESAT is planned to use a gravity gradient boom made out of nickel-titanium (Ni-Ti) wire. The Ni-Ti wire will initially be wrapped around the satellite and it will be released at peak altitude in microgravity. The balloon launch will test the release mechanism for the boom by utilizing the microgravity environment that exists after the spacecraft enters free fall. Also tested are the thermodynamic properties of different thermal surfaces on ESAT, the GaAs Solar Array, and the communications link of a Ni-Ti J-pole antenna.

The balloon launch itself will utilize unique ideas to achieve the best environment for testing ESAT. The balloon launch will make use of a smaller balloon inside of the parachute to make the decent of the satellite more linear and less chaotic.

Students of Taylor University will have access to the data collected from the launches. The small Pico-Satellite has the potential to be moved through a student's career into doctoral research, especially with its ability to explore the difficult area of the earth's atmosphere, ionosphere, and stratosphere. The balloon system benefits as we perfect it and its potential to be sold to other universities.

The whole apparatus includes a large 1000g latex weather balloon, a parachute with a smaller 100g latex weather balloon inside of it, a command pod with two regular video cameras and one high definition video camera, an accelerometer, temperature sensor, humidity sensor, and a pressure sensor. The ten meter tether is attached to the bottom of the command pod and a secondary 10 meter tether is attached to the side and wrapped around the payload (ESAT) with a 100g black and white ping pong ball attached at the end.

The balloon is filled with a small amount of gas which then expands as it ascends into the earth's atmosphere, which provides the lift we need to get the system into the stratosphere. The balloon then gets released by a cut-off switch. The system then enters a free fall which is controlled by a smaller balloon inside of a parachute, without this the command pod would fall chaotically causing unwanted vibrations and affecting the data received from the unit. The parachute does not control the descent until there is enough atmosphere to fill the parachute.

A standard definition camera will be pointed upward to watch the larger balloon's release and the parachute-balloon system. Two other cameras will be pointed toward the real mass model of ESAT and will record the tether release.

A. Payload

Command Pod:	Payload:
4in. x 4in. x 8in.	Magnetometer
Accelerometer	Solar Array
Temperature Sensor	Plasma Probe
Pressure Sensor	E-Field Detector
Humidity Sensor	VLF Receiver
Data relay	
2 video cameras	
1 HD video camera	

Table 1.1 Sensors for high altitude balloon flight.

This is a list of the sensor to be attached to the command pod and the payload (ESAT).

B. Launch Vehicle

The launch vehicle for this flight is a 1000g-1500g latex weather balloon.



C. Mission Operations Systems

The command pod is equipped with a modem which communicates with the ground directly through our J-pole antenna as it is over the United States. We can also communicate with ESAT worldwide through the Iridium Satellite constellation, owned and operated by Iridium Communications Inc. The data from ESAT is downloaded to the internet, to a tracking site located at the mission control center at Taylor University, and another tracking site at a separate location.

D. Needed Materials

Materials:
ATC3K Waterproof Action Cam (Oregon Scientific)
-48 degrees field of view
1000g latex weather balloon
100g latex weather balloon
Cut off mechanism
Parachute
Gravity Gradient tether
Command pod
-Accelerometer
-Temperature Sensor
-Pressure Sensor
-Humidity Sensor
-Data Relay
-Plasma Probe
-E-Field Detector
-VLF receiver
-Magnetometer
ESAT

Table 1.2 List of needed materials.

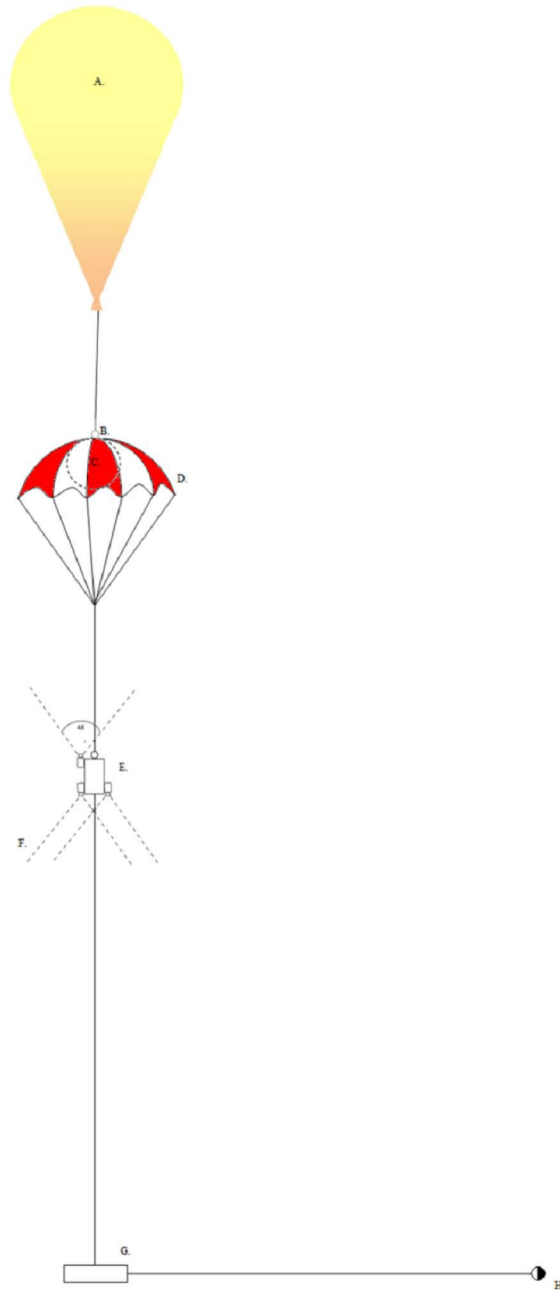


Figure 2.1 High Altitude Balloon Diagram. A.) 1000g-1500g balloon B.) Detach clip C.) Small auxiliary balloon D.) 2m diameter parachute E.) Command pod, includes Accelerometer, Temperature sensor, Pressure sensor, Humidity sensor, 2 video cameras, and 1 HD video camera F.) Camera field of view G.) ESAT H.) Ni-Ti wire tethers with painted ping pong ball on the end.

II. System Diagram

Figure 2.1 shows an illustration of the balloon system.

III. General Guidelines

The novel idea of producing power from a tether attached to the satellite by creating a potential is yet to be implemented and quantified. Our microgravity experiment seeks to prove the effectiveness of our choice of tether implementation. As has been discussed, our tether is to be wound around our satellite with a memory wire (Ni-Ti). Upon our servo release it is to unwind from the satellite and descend to an appropriate distance to create the potential desired. To visualize this process an *Interactive Physics* simulation was utilized.

In this simulation rotational springs were used to simulate the memory characteristics of our Ni-Ti wire. Rods were then used to keep the length of the wire constant. Upon winding the structure, as shown above, and running under microgravity conditions we have successfully simulated what we believe the process will look like. This is essential for understanding and visual stimulation for those trying to better understand our research.



Figure 3.2 Picture of tether release.

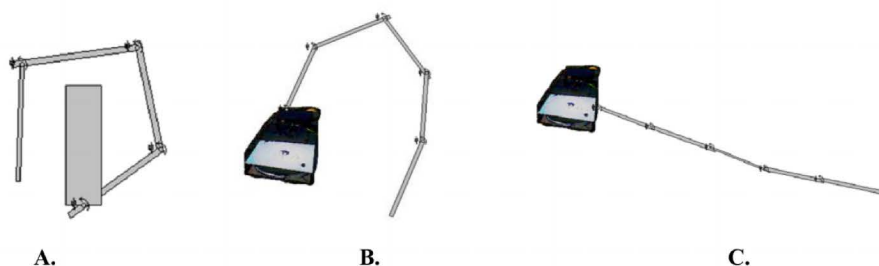


Figure 3.1 Release of the tether in *Interactive Physics*. A.) Satellite tether unwinding in initial wound condition. B.) Satellite in unwinding phase with maximum amplitude. C.) Satellite with tether fully unwound in steady state.

IV. Rotational Control

Rotational control is a powerful tool for use on satellites in orbit in controlling their attitude or stability. We will be able to model the stability control of our satellite by varying the radius of the tether and calculating the system inertia. To vary this we are able to vary the mass on the end of our Ni-Ti tether. Theoretically, we want to know how changing the boom radius will affect the system inertia and what kind of implications this has for the unwinding of our tether in the release mechanism procedure. Below are the measurements of this system:

End Mass =	100 g
Density (SAT) =	1 g/cm ³
Mass (SAT) =	880 g
Density (Ni-Ti) =	6.5 g/cm ³
Diameter (Ni-Ti) =	0.75 mm
Mass (Ni-Ti) =	18.7 g
Length (Ni-Ti) =	737.87 cm

Table 4.1 System Measurements.

Using these values and simple inertia calculations we can come up with an equation that is dependent upon radius.

$$I_{end} = \frac{mL^2}{3} \quad (1)$$

Using this inertia we can establish an approximate visual representation of how the system inertia changes as the tether changes.

unwinds, or radius

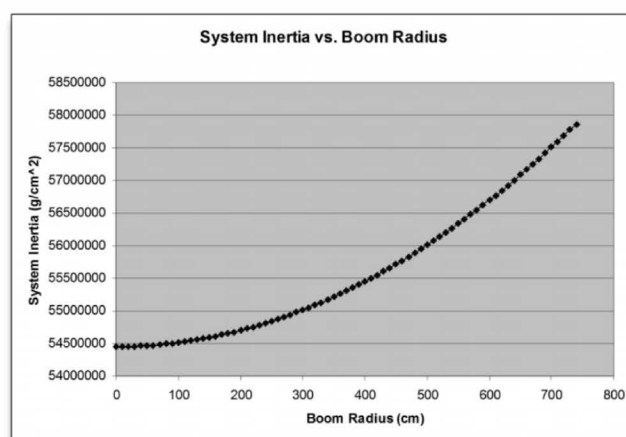


Figure 4.1 Inertia vs. Boom Radius. Being that our inertia is the medium by which we control the attitude of the satellite, we can see that our control will exponentially increase with the increase of tether radius.



V. Camera Field of View

Our camera of choice for our balloon launch is the Contour HD 1080p video camera. It utilizes a 135° wide-angle lens that delivers a true high quality image that captures all the action with minimal distortion or fish eye.

With this field of view (FOV) and knowing that our tether unwound length is 10 m we can calculate the minimum height at which we must place this camera to capture the unwinding process.

$$\tan\left(\frac{135}{2}\right) = \frac{10m}{h_{min}} \quad (2)$$

$$h_{min} = 4.1m \quad (3)$$

VI. Accelerometer

To understand the turbulence that our payload experiences throughout the duration of the flight we will be using a DE-ACCM3D2 Buffered +/- 2g Tri-axis Accelerometer. The approximate 0g reference point is at 1.66 V. With this x, y, and z direction acceleration data we can analyze the type and manner in which the module tumbles. This is specifically useful for us in trying to prove our decreased descent rate accomplished with our smaller balloon inside of our parachute and avoiding our chaotic burst by unlinking from the main balloon.

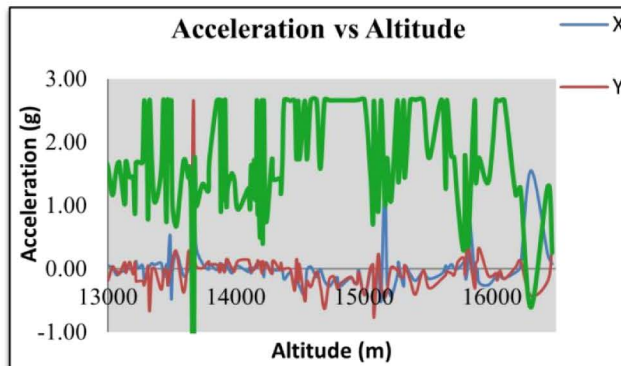


Figure 6.1 Acceleration vs. Altitude. *The results for the accelerometer data.*

and got 2.34 V. This corresponds to a 1.024g acceleration which is nearly 1 (conversion below in Eq. 4).

We can compare this descent accelerometer data with previous flights that did not have this mechanism and show the magnitude by which our average accelerations decreased and therefore the effectiveness of our descent system.

Preliminary verifications have been conducted to ensure the validity of the specifications sheet of the accelerometer. This was done by simply verifying the reference points (0 g) and then verifying response to gravity (g). Below are the results:

With zero acceleration in the z-axis direction we acquired a voltage of 1.667 V which fits the spec sheet perfectly as the reference voltage. Then we acquired data for the general acceleration due to gravity

$$G = (V - 1.66)/0.66 \quad (4)$$

These results, while difficult to read, actually show a dip in the acceleration in the vertical towards zero. This means, that for a short time, the balloon is in free-fall, and the payload experienced a zero gravity situation. This sort of environment is perfect for testing the mechanics of the tether release that will be experienced during the actual satellite flight.

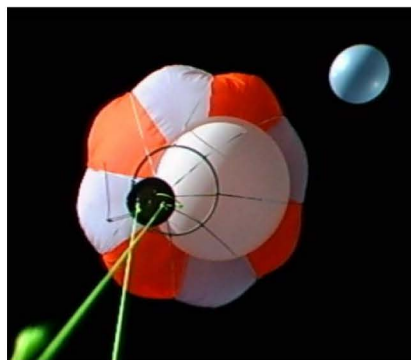


Figure 7.1 Balloon just after drop. *The smaller auxiliary balloon is seen inside the parachute and the large balloon is in the top right corner and has just been released from our system.*

VII. Balloon Controlled Decent

One of the novel ideas on this balloon launch is the balloon parachute system. A small 100 gram balloon is placed inside the parachute to allow for smooth post burst descent. This post burst control creates ideal conditions for the microgravity experiment. For this system the balloon must be sufficiently filled in order to assist in slowing descent but it must not be so filled that it overinflates and pushes against the parachute.

In order to make sure that the small balloon doesn't expand to be larger than 4 feet inside of the parachute, the balloon must be filled to a proper volume of $3.34 \times 10^{-2} m^3$ on the ground. For calculations see the appendix.

The controlled descent was a success. The balloon system remained fully vertical after release of the large balloon. A few seconds of microgravity were achieved as we can see in the accelerometer data in the appendix, the z-axis accelerometer reading drops significantly at the release of the balloon.

These results, while difficult to read, actually show a dip in the acceleration in the vertical towards zero. This means, that for a short time, the balloon is in free-fall, and the payload experienced a zero gravity situation. This sort of environment is perfect for testing the mechanics of the tether release that will be experienced during the actual satellite flight.

VIII. J-Pole Antenna

For our communication between our command pod with the control center on the ground, we used a J-Pole antenna. J-Pole antennas were originally designed and used on Zeppelins and other balloon equipment, so it fits perfectly that we use it on our balloon experiment. J-Poles are also the ideal choice in this situation because they are a unidirectional dipole antenna, and can be easily manufactured for any range of frequencies. There are many J-Pole calculators on the web, which take the required frequency that the J-Pole will accept, and outputs the exact lengths of every dimension of the antenna. Our command pod used a frequency of around 915 MHz, and when put into a J-Pole calculator gives us these results:

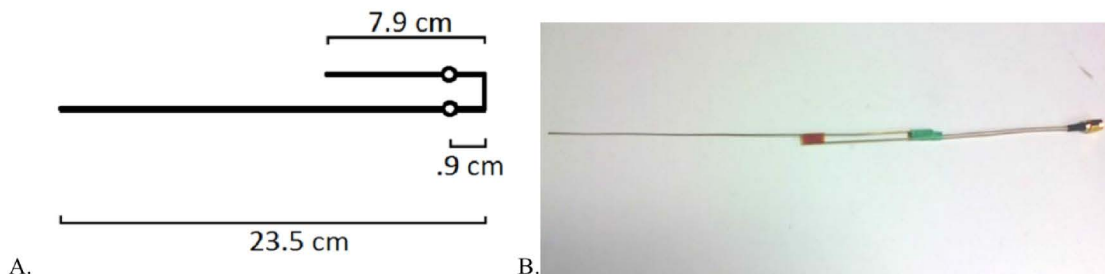


Figure 8.1 J-Pole Antenna. A.) J-Pole Design Spec. B.) Photo of J-Pole Antenna

IX. Thermal Model Test

This balloon is testing the heat transfer, by radiation, of various materials. This experiment will help to decide the thermal surfaces most appropriate for ESAT. The layout of ESAT is given in Figure 9.1 and shown in Figure 9.2

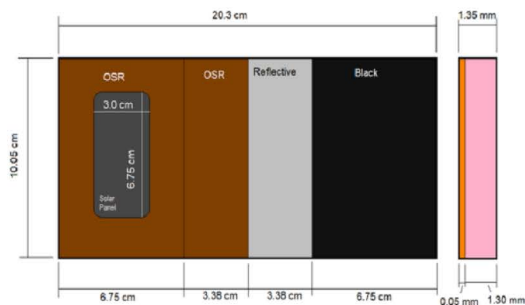


Figure 9.1 Diagram of thermal surfaces on ESAT.



Figure 9.2 ESAT with thermal surfaces.

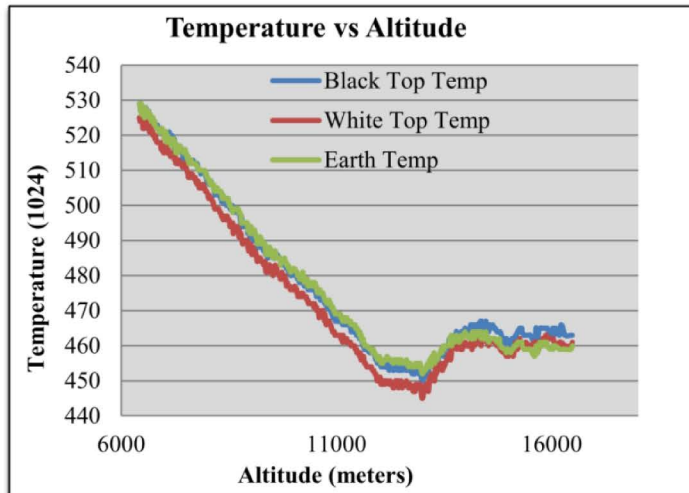


Figure 9.3 Thermal Results from balloon launch

This system contains three different surfaces with a temperature gauge per surface. One of the surfaces will also house a solar panel, which is discussed more under the Solar Panel Analysis section. Figure 9.2 shows the final design of the Thermal Model Test, along with the surfaces and the solar panel in place.

Our goal for this test was to see which surface would reflect the most heat, in order to keep ESAT at an appropriate temperature. Our three surfaces were a solar panel, a metal surface painted black and a metal surface painted white. From gathering the data, we were able to find the differences in temperature between the individual materials and the temperature of the air surrounding ESAT. Our way of

analyzing this information was by summing the differences of temperature for each material and compare.

After reviewing the data, the surface which was painted white had the least change in temperature from the air surrounding the pod. We felt that this material would properly protect ESAT from becoming too hot from the sun's radiation.

X. Solar Panel Analysis

We want to test the peak voltage and current of our solar panel, so that we can best utilize it on the satellite. We will accomplish this by attaching a resistor of known resistance and monitoring voltage. In this way, we will be able to keep track of both current and voltage throughout the course of a balloon flight, during which we will surely experience both greater voltages and currents than experienced at ground level.

To maximize the efficacy of this test, an appropriate resistor size must be chosen. We decided to pick a resistor that matches the V-I characteristics of the peak power of the panel.

From the data sheet:

$$J_{mp} = 14.15 \frac{mA}{cm^2} \quad (5)$$

$$V_{mp} = 2.085 V \quad (6)$$

$$A = 6.9 cm * 3.9 cm = 26.9 cm^2 \quad (7)$$

So, for this size solar panel, the maximum power corresponds to a current of:

$$I_{mp} = 14.15 \frac{mA}{cm^2} * 26.9 cm^2 = 381 mA = 0.381 A \quad (8)$$

With a voltage of $V_{mp} = 2.085 V$, this corresponds to a characteristic resistance of:

$$R_{mp} = \frac{V_{mp}}{I_{mp}} = \frac{2.085 V}{0.381 A} = 5.48 \Omega \quad (9)$$

For the sake of this experiment, a 5.1Ω resistor was used, to guarantee that the voltage sensor was not potentially overloaded with current. Using this, we were able to wire up the circuit (Figure 10.1).

Using this circuit, we can monitor voltage and current from a typical solar cell at high altitudes, and we will be able to use this information for calibrating solar cell usage on the actual satellite.

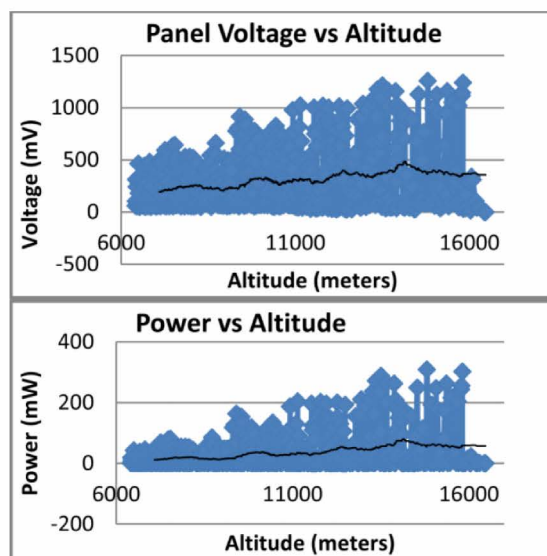


Figure 10.2 Solar Panel Results. The black line in each graph represents the average.

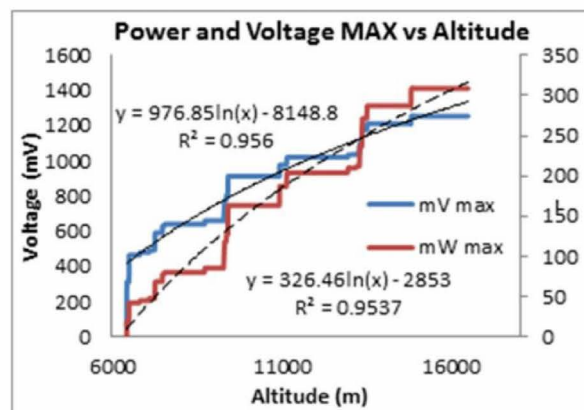


Figure 10.3 These graphs show a definite increase in both power and altitude. Voltage increases by almost a factor of three over and altitude change of about 10 km, while power increases by a factor of six. This is a surprising increase in efficacy of the solar panel with altitude.

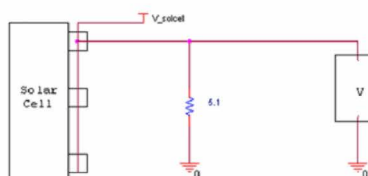


Figure 10.1 Solar Circuit Diagram.

A. Solar Panel Results

Measuring voltage and current and power produced by the solar panel during the balloon flight yielded the following results in Figure 10.2.

These results demonstrate a lot of noise and may reflect turbulent motion during the balloon ascent. A reasonable assumption to make, then, is that the maximum values reflect when the solar panel was oriented directly toward the sun. Since this will be the orientation during the duration of the actual satellite flight, isolating these values should give a better view of what the voltage and power will be during the actual satellite flight, see Figure 10.3.

Using the trend provided by the graphs, the voltage and power expected at 200 km (the height of the actual satellite flight) might be extrapolated:

$$V_{mV} = 977 * \ln|Alt| - 8150 \quad (10)$$

$$V_{mV} = 977 * \ln|200,000 m| - 8150 = 3780 mV = 3.78 V$$

$$P_{mW} = 326 * \ln|Alt| - 2853 \quad (11)$$

$$P_{mW} = 326 * \ln|200,000| - 2853 = 1130 mW = 1.13 W$$

From these values, we should be able to determine, to a reasonable degree, the power we can expect from the solar panels during the flight of the satellite.

XI. Conclusion

The main objective of this balloon launch was to test the release of a ten meter boom in microgravity (free fall) at 25 km altitude. The successful release and unraveling of the tether will be a monumental achievement in the area of Pico-Satellite capabilities. In addition to the ten meter boom, a new design of inserting a smaller balloon inside of the parachute for a less chaotic decent in free fall has been implemented with success. Microgravity is an important environment for experimentation. There is a short period of microgravity after the payload is dropped before resistive forces become significant. Microgravity gives an opportunity to test equipment in roughly zero Gs with only a few percent of the Earth's atmosphere. This project tested a real mass model satellite and attempted to optimize a balloon launch for space environment testing, with varying degrees of success.

Other important experiments included in this launch consisted of the GaAs Solar Array Testing, Thermal Surface Model Testing, Communications link tested with a new nickel-titanium wire J-pole antenna and a Tether Release Model computer simulation that was compared to the actual experimental execution of the tether release. All of these experiments gathered useful information that both furthers our knowledge of the upper atmosphere and provides incredibly useful insight for the design and implementation of the pico-satellite.

Appendix

A. Calculations on Heat loss and Thermal surfaces for ESAT 2

We start with the following assumptions:

Bottom of satellite pointed toward Earth

Everywhere else pointed toward black space

Sun hits one solar paneled side directly on

1. Heat – losing capacity

$$\frac{P}{A} = \epsilon\sigma(T^4 - T_c^4) \quad (12)$$

Where P = power, ϵ = emissivity, σ = Stefan constant, A = area, T = temp, T_c = cooler temp

We calculated the incident radiation from the sun, using the following equation:

$$P = A_{sun}\epsilon\sigma(T_{sun}^4 - T_{sat}^4) * \frac{A_{sat}}{A_{AU}} \quad (13)$$

Where A_{sun} = surface area of the sun, A_{sat} = area of satellite, A_{AU} = area of sphere of radius 1 AU

According to the excel, the equilibrium temperature of the satellite in the sun, with no internal power, is approximately $T \approx 10^\circ$ F.

With a load of 100 W, however, the temperature will rise to about $T \approx 320^\circ$

2. Heat Transfer

The formula for heat transfer is:

$$\frac{P}{A} = \epsilon\sigma(T_H^4 - T_C^4) \quad (14)$$

Assuming the panels are facing the sun, the temperatures reached by the different panels will be found using:

$$\epsilon\sigma(T_{sat}^4) * A_{panel} = abs * \sigma(T_{sun}^4 - T_{sat}^4) * \frac{D_{sun}}{D_{earth}} * A_{panel} \quad (15)$$

$$\epsilon * T_{sat}^4 = a * \frac{D_s}{D_e} * T_{sun}^4 - a * \frac{D_s}{D_e} * T_{sat}^4 \quad (16)$$

$$T_{sat}^4 = \frac{a * \frac{D_s}{D_e} * T_{sun}^4}{\epsilon - a * \frac{D_s}{D_e}} \quad (17)$$

$$T_{sat} = \sqrt[4]{\frac{a * \frac{D_s}{D_e} * T_{sun}^4}{\epsilon - a * \frac{D_s}{D_e}}} \quad (18)$$

$$\frac{D_e}{D_s} = \frac{6.955 * 10^8 \text{ m}}{1.496 * 10^{11} \text{ m}} = 4.65 * 10^{-3} \quad (19)$$

$$T_{sun}^4 = (5778 \text{ K})^4$$

$$T_{sat} = 1509 * \sqrt[4]{\frac{a}{\epsilon - a * 4.65 * 10^{-3}}} \quad (20)$$

$$T_{sat} \approx 1500 * \sqrt[4]{\frac{a}{\epsilon}} \quad (21)$$

According to this equation, the black part should get very hot, close to 2000 °F, while the OSR and the reflective tape should get very cold.

The solar panel section should be about:

$$T_{panel} = 1500 * \sqrt[4]{\frac{0.7 * 0 + 0.3 * 0.92}{.7 * 1 + 0.3 * 0.8}} \approx 1000 \text{ °F} \quad (22)$$

This is for ideal characteristics, however. It will be interesting, however, to see the actual temperature variation.

B. Balloon Controlled Descent Calculations

In order to make sure that the small balloon doesn't expand to be larger than the inside of the parachute, we must calculate the volume with which to fill the balloon on the ground. To do this we use the ideal gas law since helium is



an ideal gas. This law is $pV=nRT$, in which p is pressure, V is volume, n is the amount of gas, R is the ideal gas constant, and T is the absolute temperature. The max diameter for the expansion of the balloon is 4 ft, which gives us a max volume of (using $V = \frac{4}{3}\pi r^3$) of

$$V = 33.51032164 \text{ ft}^3$$

$$V = 0.948906637 \text{ ft}^3$$

Knowing the pressure and temperature at 80,000 ft:

$$P_{80} = 2798.4362 \text{ Pa}, \quad T_{80} = 220.788 \text{ K}$$

and at ground level:

$$P_g = 98427.756 \text{ Pa}, \quad T_g = 295 \text{ K}$$

we can then calculate V_g and r_g .

Knowing

$$PV = nRT \tag{23}$$

we have,

$$nR = \frac{P_1 V_1}{T_1} = \frac{P_2 V_2}{T_2} \Leftrightarrow V_1 = \frac{T_1 P_2}{T_2 P_1} V_2 \tag{24}$$

$$\frac{4}{3}\pi r_1^3 = \frac{T_1 P_2}{T_2 P_1} * \frac{4}{3}\pi r_2^3 \tag{25}$$

$$r_1 = \left(\frac{T_1}{T_2} * \frac{P_2}{P_1}\right)^{\frac{1}{3}} r_2 \tag{26}$$

We can now calculate:

$$V_{ground} = 0.033426469 \text{ m}^3$$

$$V_{ground} = 1.180444612 \text{ ft}^3$$

This gives us a radius and diameter on the ground of:

$r_g =$	0.204060096	m
$r_g =$	0.669488507	ft
$d_g =$	0.408120193	m
$d_g =$	1.338977013	ft

Table A.1 Ground radius and diameter.

C. Inertia of Boom Calculations

Knowing the mass of the weights, material of the rod, and density and dimensions of the rod we can calculate the moment of inertia of the system by adding the inertias of each individual part of the system. For a solid cube, such as our magnets and our approximation of the satellite, the moment of inertia can be calculated as:

$$I_w = \frac{1}{12} m(h^2 + d^2) \tag{27}$$

The moment of inertia for the rod with a mass at the end can be calculated as:

$$I_{end} = \frac{mL^2}{3} \tag{Eq. 1}$$

Then assuming a density of water for our satellite and knowing its dimensions to be 20.32 cm x 10.16 cm x 3.38 cm we can calculate our satellites mass. Upon calculation we get that our cube, rod, and magnets have moments of inertia as follows:

	Magnet Mass (g*cm ²)
I_{cube}	6662.688352
I_{rod}	9572040.116
I_{mags}	4890375.204
I_{total}	14469078.01

Table A.2

I_{magn}	Total Inertia (kg*cm ²)
6662688.63	16241.39143
66626886.3	76205.5891
333134431.5	342713.1343
666268863	675847.5658
1332537726	1342116.429
1998806589	2008385.292
2665075452	2674654.155
3331344315	3340923.018
3997613178	4007191.881
4663882041	4673460.744
5330150904	5339729.607
5996419767	6005998.47
6662688630	6672267.333

Table A.4 As expected, the plot is linear showing that the more mass we add to the end of our rod, the more resistance/control we will gain in our satellite orbit.

Then, in order to plot the system moment of inertia vs. the mass at the end of the rod we tabulate the magnet mass as a fraction of the actual satellite mass as follows:

	Magnet Mass
.1% cube	6.662688352
1% cube	66.62688352
5% cube	333.1344176
10% cube	666.2688352
20% cube	1332.53767
30% cube	1998.806506
40% cube	2665.075341
50% cube	3331.344176
60% cube	3997.613011
70% cube	4663.881847
80% cube	5330.150682
90% cube	5996.419517
100% cube	6662.688352

Table A.3

With this we can calculate the new moments of inertia of these “end masses” and plot it against the total inertia of the system to see what kind of resistances we will be dealing with by applying differing loads.

D. Magnetic Torque Calculations

Magnetic torque between magnetic field and a bar magnet can be calculated with the following equation:

$$\tau = m \times B \quad (28)$$

Where m = magnetic moment and B = magnetic field

And $m = p * l$

Where p = strength of a pole and l = length of bar magnet

And $p = B_b * A$

Where B_b = magnetic strength of bar magnet and A = cross sectional area of the bar magnet

Assuming a bar magnet length of about 10 cm and a cross sectional area of 1 square cm.

Also assuming maximum torque, where the bar magnet and b-field are perpendicular:

$$\tau = m * B$$

We will take the earth’s magnetic field to be about 0.5 gauss = 50 uT.

We are looking for a torque of about 0.5 N m.

Substituting and solving for B_b , we can find what the field strength of the bar magnet needs to be.

$$B_b = \frac{\tau}{B * l * A} \quad (29)$$

$$B_b = \frac{0.7 \text{ J}}{50 \mu\text{T} * 1 \text{ m} * 0.0001 \text{ m}^2} = 14 \quad (30)$$

Unfortunately, this kind of magnetic field from a bar magnet is unreasonable. For this flight, my suggestion is to put on as many magnets as possible, and hope that the small force, coupled with the moments inertia of the magnets and the lever arms, keep the balloon stable.

E. Infrared Radiation Throughout the Troposphere and Stratosphere

I. Introduction

This payload will measure the infrared (IR) radiation present at different altitudes in earth’s atmosphere. Three different IR sensors, each with a filter that passes a different band of the IR spectrum, will be mounted on a structure that will be flown up to an altitude of 100,000 feet on a high altitude balloon. This will allow for a detailed analysis of the amount of solar IR radiation permitted through the atmosphere to different altitudes, both for radiation that comes directly from the sun and for radiation from the sun that is scattered by the atmosphere.

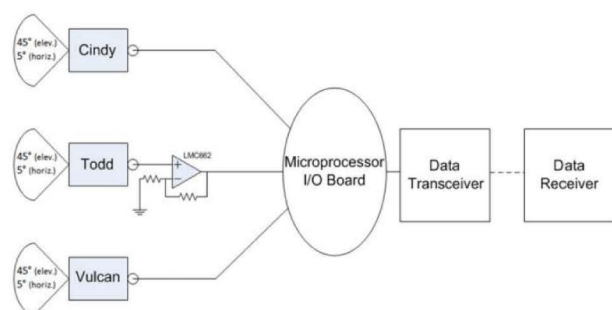


Figure A.2 System Layout Diagram.

canister to allow the three sensors to aim at the solar zenith, and this slit will contain a collimator.

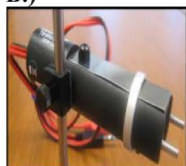
In addition to the sensors themselves, other electronic components will be flown inside the canister. A



A.)



B.)



C.)



D.)

Figure A.2 Sensor Detail Photos. A.) Cindy (bottom) and Todd (top). B.) Inputs and Outputs: (L→R) Cindy input, Cindy output, Todd input. (Todd's output is a pair of banana plugs. C.) Mounting Mechanism for Todd. D.) Structure of balloon canister. Note that the experiment mounted onto the canister is not the infrared experiment discussed in this paper.

⁷Source: <http://store.pasco.com/>

⁸Source: ***manual needed***

2. System Overview and Physical Description

All the components of this system (obviously except the data receiver) will be mounted inside one balloon launch canister. The canister is a cylinder such as the ones typically used in the Taylor High Altitude Balloon program. Todd will be mounted on the canister interior's supporting rod using its screw mechanism and securing adhesives or wire ties. Because of their small size, Cindy and Vulcan will be mounted directly onto Todd using strong tape or wire ties. As discussed below in the "Sensor Orientation" section, a slit will be cut in the side of the

microcontroller will process the data from the three sensors, and a transceiver will send that data to ground control at a rate of about one data set per second. Cindy and Vulcan will output directly to the microcontroller, but Todd's signal will be amplified by an op-amp before reaching the microcontroller.

3. Sensor Specifications

The three IR sensors on this payload have the following specifications:

"Cindy" (Pasco CI-6628)

Sensing Element⁷: 48 junction, KRS-5 window, argon gas-filled thermopile

Spectral Response⁷: 700-30,000 nm (optimal), 600-40,000 nm (total)

Output Voltage⁷: 0-5 V

"Todd" (Pasco TD-8553)

Sensing Element⁷: Dexter 2M

Spectral Response¹: 600-30,000 nm (flat spectral response)

Output Voltage⁷: ****

"Vulcan" (**details yet to be found**)

Sensing Element⁸: ****

Spectral Response⁸: ****

Output Voltage⁸: ****

4. Filtration

Each sensor will be equipped with a filter which will pass only a specific band of IR radiation. In this way, the three sensors will each measure a different band of the IR spectrum. The readings obtained by each sensor will thus be the sum of all the radiation in its frequency band; this sum is

mathematically equivalent to Wien's law for the black body integrated over the frequency range observed. The three sensors will be filtered for the following bands of IR radiation:

- Cindy: ****_**** nm (**wavelengths yet to be determined**)
- Todd: ****_**** nm
- Vulcan: ****_**** nm

5. Calibration

The data generated by each sensor will consist of relative intensities of IR radiation. Before the flight, the three sensors will be calibrated by comparing their readings to those of a spectrometer. Each of these four instruments will be used to measure the radiation levels of two different black bodies: the sun (as seen from ground level) and an incandescent light bulb. The IR sensors' readings of relative IR intensity will be compared to the spectrometer's readings of absolute IR intensity for these two black bodies. If we assume that each IR sensor responds linearly to increased IR intensity, this comparison will generate a conversion factor to convert each sensor's relative readings to absolute readings. Thus, we can use the relative IR intensities measured during the balloon flight to obtain the absolute IR intensities detected throughout the atmosphere.

6. Sensor Orientation

When the sensors are flown, they will be aimed at 45° from vertical; this is approximately the solar zenith angle around the time of flight⁹. The light will be collimated for the sensors by a thin slit; the slit will allow a 5° horizontal FOV and a 45° elevation FOV. As the payload rotates freely under the balloon, the sensors will be aimed at the sun once per rotation. The large elevation FOV allows the sun's radiation to be observed even if the payload bounces throughout its flight; and the small horizontal FOV blocks the sun's radiation for most of the rotation cycle, thus allowing for much data from the scattered atmospheric radiation.

In this way, the sensors will study both the radiation coming directly from the sun and the radiation scattered by the atmosphere. It will be relatively simple to decide which data points measure the sun's direct IR radiation and which are not--the sun's direct radiation should be much more saturated than the atmosphere's scattered IR radiation.

Acknowledgments

All authors would like to thank faculty advisors Hank D. Voss¹⁰ and Jeff F. Dailey¹¹.

References

Interactive Physics Software Program, <http://www.design-simulation.com/IP/index.php>, Design Simulation Technologies, Inc., Canton, MI

Holmes, W.C., J. Bryson, B. Gerig, J. Oehrig, J. Rodriguez, J. Schea, N. Schutt, D. Voss, J. Voss, D. Whittington, A. Bennett, C. Fennig, S. Brandle, J. Dailey, H.D. Voss, TU Sat 1: A Novel Communications and Scientific Satellite, 16th Annual/ USU Conference on Small Satellites, 2002.

⁹ The solar zenith angle was computed using <http://solarat.uoregon.edu/SolarPositionCalculator.html> to be 50.87° at 10:30 am (the planned launch time). This angle was checked using http://www.sunearthtools.com/dp/tools/pos_sun.php, which computed the solar elevation to be 39.12° (thus, the solar zenith angle was 90° - 39.12° = 50.88°. These calculations used the following inputs: Upland, Indiana (40.4755974 N, 85.4944168 W); April 20, 2011, 10:30 am; Eastern Daylight Time (GMT -4). Similarly, the solar zenith angle was computed to be 45.67° at 11:00 am and 40.81° at 11:30 am.

¹⁰ Professor, Physics and Engineering Department, 236 W. Reade Ave.

¹¹ Professor, Physics and Engineering Department, 236 W. Reade Ave.